Optics Communications 388 (2017) 53–61

Contents lists available at ScienceDirect

Optics Communications

journal homepage: www.elsevier.com/locate/optcom

Comparative assessment of astigmatism-corrected Czerny-Turner imaging spectrometer using off-the-shelf optics

Qun Yuan[a,*], Dan Zhu[a], Yueyang Chen[a], Zhenyan Guo[a], Chao Zuo[a,b], Zhishan Gao[a]

[a] Nanjing University of Science and Technology, School of Electronic and Optical Engineering, Xiaolingwei 200#, Nanjing 210094, China
[b] Nanjing University of Science and Technology, Jiangsu Key Laboratory of Spectral Imaging & Intelligence Sense, Xiaolingwei 200#, Nanjing 210094, China

ARTICLE INFO

Keywords:
Spectrometer
Aberration
Field of view
Off-the-shelf
Distortion

ABSTRACT

We present the optical design of a Czerny-Turner imaging spectrometer for which astigmatism is corrected using off-the-shelf optics resulting in spectral resolution of 0.1 nm. The classic Czerny-Turner imaging spectrometer, consisting of a plane grating, two spherical mirrors, and a sensor with 10-μm pixels, was used as the benchmark. We comparatively assessed three configurations of the spectrometer that corrected astigmatism with divergent illumination of the grating, by adding a cylindrical lens, or by adding a cylindrical mirror. When configured with the added cylindrical lens, the imaging spectrometer with a point field of view (FOV) and a linear sensor achieved diffraction-limited performance over a broadband width of 400 nm centered at 800 nm, while the maximum allowable bandwidth was only 200 nm for the other two configurations. When configured with the added cylindrical mirror, the imaging spectrometer with a one-dimensional field of view (1D FOV) and an area sensor showed its superiority on imaging quality, spectral nonlinearity, as well as keystone over 100 nm bandwidth and 10 mm spatial extent along the entrance slit.

1. Introduction

The Czerny-Turner imaging spectrometer, in which a plane grating and two spherical mirrors are configured in a coma-free geometry with the Shafer equation satisfied, is commonly used to resolve spectral intensity [1,2]. In addition, spherical aberration can be limited if the spectrometer has a low numerical aperture. However, off-axis reflections from the collimating and focusing spherical mirrors of the classic Czerny-Turner imaging spectrometer introduce astigmatism, thus preventing the spectrometer from achieving high resolution. Sub-nanometer spectral resolution is necessary for remote sensing [3], spectrally resolved white light interferometry [4], and Fourier domain optical coherence tomography (FD-OCT) [5].

Astigmatism in the classic Czerny-Turner imaging spectrometer can be reduced or removed by compensating the focal lengths of the mirrors in the tangential and sagittal planes. This can be done by adding elements such as a cylindrical lens [6], a cylindrical mirror [7], a tilted parallel plate [8], a small piece of glass using as a 1D waveguide [9], a toroidal lens [10], or a customized lens [11], or one more mirror to change to the Schwarzschild spectrometer [12]; changing one element, e.g., using a convex grating [13], and using a toroidal focusing mirror [14,15]; or introducing divergent illumination by minimizing the distance between the input entrance slit and the collimating mirror [16]. With the development of new design methods of freeform optics [17,18], spectrometer designs that leverages freeform surfaces have been reported [19]. Lee et al. [6] reported on a spectrometer with a linear sensor of 8000 pixels and a cylindrical lens that achieved a spectral resolution of better than 0.1 nm over a bandwidth of 400 nm. A fiber or a pinhole delivers light to the entrance of this spectrometer for use in an FD-OCT system. Their spectrometer employs a zero-dimensional spot or point FOV, providing only spectral discrimination. Others have shown astigmatism correction over some bandwidth and transverse spatial extent [7,14,15] using a spectrometer with an area sensor that provides not only spectral but also spatial discrimination. In some scanning methods, a whiskbroom scanning instrument employs an imaging spectrometer with a point FOV that scans the object in both the along-track and cross-track directions, while in other scanning methods, a pushbroom scanning instrument employs an imaging spectrometer with a one-dimensional (1D) FOV that scans in only one direction [20].

Different pursuance for correcting astigmatism in the Czerny-Turner imaging spectrometer have been made, including the use of an extended spectral range, high spectral resolution, and spatial extent. In this paper, we comprehensively compare different modifications of

* Corresponding author.
E-mail address: karmen86913@gmail.com (Q. Yuan).

http://dx.doi.org/10.1016/j.optcom.2016.11.004
Received 5 October 2016; Received in revised form 30 October 2016; Accepted 1 November 2016
Available online 17 November 2016

the benchmark classic Czerny-Turner imaging spectrometer to obtain ultrahigh resolution using only cost-effective off-the-shelf optics, so any customized optics, such as toroidal lens or mirror, freeform surfaces will not be taken into account. We comparatively assessed three configurations for astigmatism correction of the spectrometer: one using divergent illumination of the grating, one with an added cylindrical lens, and one with an added cylindrical mirror.

For our study, the targets of 0.1-nm spectral resolution and a 10-μm pixel size were fixed conditions, so the detector was chosen with respect to the parameters of spatial extent and spectral range. The radii of the collimating and focusing spherical mirrors and the parameters of the plane grating were the same for all three configurations. In Section 2, we discuss the principles and methods of astigmatism correction. In Section 3, techniques and schemes for astigmatism correction along spectral and spatial directions are compared. In Section 4, designs of the three configurations with the same parameters and with off-the-shelf optics, and their performance with respect to the maximum allowable wavelength bandwidth, spectral nonlinearity, smile, and spectral keystone are evaluated. The suggestions for design of our astigmatism-corrected Czerny-Turner imaging spectrometer and our conclusions are summarized in Section 5.

2. Principles

2.1. Classic Czerny-Turner imaging spectrometer

The classic Czerny-Turner imaging spectrometer is illustrated in Fig. 1. A divergent beam from the entrance pinhole or slit is reflected by the collimating mirror and then diffracted in the tangential plane by the plane grating. The focusing mirror focuses the dispersed beam onto the detector. If the beam enters through a pinhole, a linear sensor captures the spectral information, thus giving the imaging spectrometer a configuration with a point FOV. If the beam enters through a slit, an area sensor captures both the spectral and spatial information, thus giving the imaging spectrometer a configuration with a 1D FOV.

The spherical aberration introduced by the collimating and focusing spherical mirrors can be derived from the *f*-number. Therefore, the Rayleigh criterion can be the design criterion for constraining the *f*-number to achieve limited diffraction.

Coma aberration is corrected when the geometry of the spectrometer satisfies the Shafer equation [2]:

$$\frac{\sin\alpha_1}{\sin\alpha_2} = \left(\frac{R_1}{R_2}\right)^2 \left(\frac{\cos\theta\cos\alpha_1}{\cos i\cos\alpha_2}\right)^3, \tag{1}$$

where α_1 and α_2 are the angles of incidence of light on the collimating mirror and the focusing mirror, respectively; R_1 and R_2 are the radii of the collimating mirror and the focusing mirror, respectively; θ is the diffraction angle of the grating; and i is the angle of incidence of light on the grating. The relationship between i and θ is shown in Fig. 1 and is determined by the groove interval d of the grating, expressed in Eq. (2):

$$d(\sin i + \sin\theta) = m\lambda \tag{2}$$

where the diffraction order m=−1. The collimated beam is dispersed spectrally by the grating and the angular spectral spread $\Delta\theta$ is given by

$$\Delta\theta = \left(\frac{\mathrm{d}\theta}{\mathrm{d}\lambda}\right)\Big|_{\lambda=\lambda_0} \bullet\Delta\lambda = \frac{\Delta\lambda}{\mathrm{d}\cos\theta_0} \tag{3}$$

where $\Delta\lambda$ is the wavelength bandwidth centered at λ_0 and θ_0 is the diffraction angle at λ_0. The spatial length L of the detector is then determined by $\Delta\theta$ and radius R_2 of the focusing mirror:

$$L = R_2\Delta\theta/2. \tag{4}$$

When the spectral resolution and the pixel size are fixed, as in this study, $\Delta\theta$ is larger over a broadband bandwidth $\Delta\lambda$ and L is longer in the spectral direction. In addition, over a broadband bandwidth $\Delta\lambda$, the difference in θ will be larger, thus making it difficult to satisfy Eq. (1), and then coma correction will be a problem.

Astigmatism due to the different foci for the off-axis mirrors in the sagittal and tangential planes is an inherent limitation of the classic Czerny-Turner imaging spectrometer. It is reduced or eliminated by compensating the focal lengths of the mirrors in the tangential and sagittal planes. We will only discuss the measures using cost-effective off-the-shelf optics to achieve this goal.

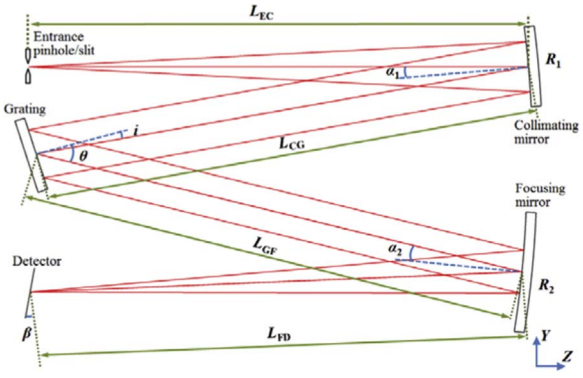

Fig. 1. Classic Czerny-Turner imaging spectrometer: L_{EC} is the distance from entrance pinhole or slit to the collimating mirror of radius R_1 and off-axis incident angle α_1; L_{CG} is the distance from the collimating mirror to the grating, which has incident angle i and diffraction angle θ; L_{GF} is the distance from the grating to focusing mirror of radius R_2 and off-axis incident angle α_2; and L_{FD} is the distance from the focusing mirror to the detector, tilted at an angle β.

2.2. Configuration with divergent illumination of the grating

One way for astigmatism correction is to get divergent illumination onto the plane grating by reducing the distance between the entrance pinhole or slit and the collimating mirror (L_{EC}) [16]. The configuration is the same as that of the classic Czerny-Turner imaging spectrometer shown in Fig. 1, but it avoids the need for complex optics such as a nonspherical mirror and aplanar grating. In the sagittal plane, the plane grating acts like a mirror, and in the tangential plane, diffraction from the grating introduces astigmatism that can compensate for that induced by the off-axis spherical mirrors.

Zero-order divergent illumination condition occurs for astigmatism correction at one specific wavelength when the distance from the entrance pinhole or slit to the collimating mirror, L_{EC}, and the distance from the focusing mirror to the detector, L_{FD}, are defined as follows [16]:

$$L_{EC} = \frac{R_1R_2\left(\frac{\cos^2 i}{\cos^2\theta} - 1\right)/2}{R_1(\sec\alpha_2 - \cos\alpha_2) + R_2\left(\frac{\cos^2 i}{\cos^2\theta}\sec\alpha_1 - \cos\alpha_1\right)}, \tag{5}$$

$$L_{FD} = \frac{R_1R_2L_{EC}}{2L_{EC}(R_1\cos\alpha_2 + R_2\cos\alpha_1) - R_1R_2}. \tag{6}$$

However, both θ and α_2 are wavelength dependent. Furthermore, the intersection of the light rays with the focusing mirror moves as the wavelength changes, which changes L_{FD}. As θ changes, the derivative that represents the variation of α_2 and L_{FD} are expressed respectively as

$$\frac{\mathrm{d}\alpha_2}{\mathrm{d}\theta} = 1 - \frac{L_{GF}}{R_2\cos\alpha_2}, \tag{7}$$

$$\frac{\mathrm{d}L_{FD}}{\mathrm{d}\theta} = \tan\beta\left(L_{GF} + L_{FD} - \frac{2L_{GF}L_{FD}}{R_2\cos\alpha_2}\right) - L_{GF}\tan\alpha_2, \tag{8}$$

where L_{GF} is the distance from the grating to the focusing mirror and β is the angle of the tilted detector; both parameters are constrained. A

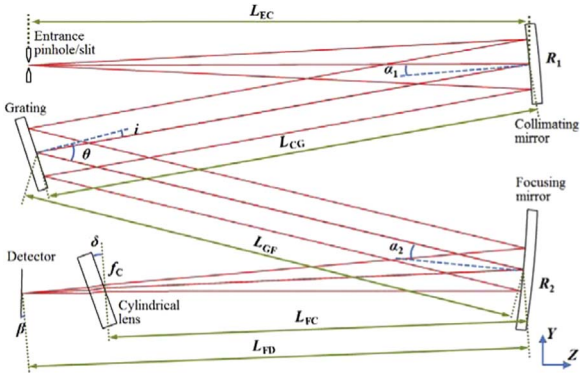

Fig. 2. Modified Czerny-Turner imaging spectrometer with a cylindrical lens of focal length f_C in the sagittal plane, tilted δ to the beam, inserted between the focusing mirror and the detector. The distance from the focusing mirror to the cylindrical lens is L_{FC}.

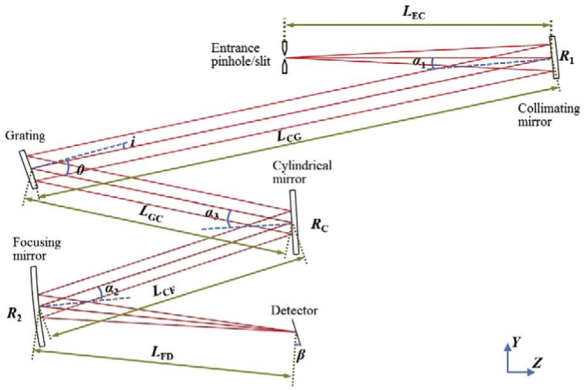

Fig. 3. Modified Czerny-Turner imaging spectrometer with a cylindrical mirror of radius R_C in the sagittal plane and at an off-axis incident angle α_3 in the tangential plane, inserted between the grating and the focusing mirror. The distance from the grating to the cylindrical mirror is L_{GC} and that from the cylindrical mirror to the focusing mirror is L_{CF}.

stigmatic image is maintained when L_{GF} and β satisfy the first-order condition of Eqs. (7) and (8). [Eq. (7) is from Austin et al. [16], in their paper, they denote the diffraction angle from the grating as β, whereas we use θ.] This configuration with divergent illumination of the grating eliminates astigmatism to the first-order wavelength using only the optics in the classic Czerny-Turner imaging spectrometer.

2.3. Configuration with an added cylindrical lens

Astigmatism in the classic Czerny-Turner imaging spectrometer can be defined by the difference of foci in the sagittal and tangential planes:

Astigmatism is corrected by inserting a cylindrical lens, with focal length f_c, central thickness t, and refractive index n, between the focusing mirror and the detector, as shown in Fig. 2. In the tangential view, the cylindrical lens works as a plane parallel plate, and in the sagittal view, it works as a lens with focal length f_c. To correct astigmatism at a specific wavelength, the cylindrical lens should be positioned such that the distance from the focusing mirror to the lens, L_{FC}, is defined as [6]

$$L_{FC} = \frac{R_2 \cos\alpha_2}{2} - \frac{P}{2} - \frac{\sqrt{P^2 + 4Pf_C}}{2} - t, \tag{10}$$

where $P=\Delta f - t(n-1)/n$. The off-axis angle α_2 incident to the focusing mirror varies with the wavelength because of the diffraction. The variation across the focusing mirror results in the variation of astigmatism, Δf, across the detector. This nonuniform astigmatism for different wavelengths can be compensated by tilting the cylindrical lens at an angle δ and tilting the detector at an angle β. The two optimized angles are calculated using Eq. (14) from Lee et al. [6].

2.4. Configuration with an added cylindrical mirror

Astigmatism in the classic Czerny-Turner imaging spectrometer can also be defined by the difference of optical power in the sagittal and tangential planes:

$$\begin{aligned}\Delta\Phi &= \Phi_{T1} - \Phi_{S1} + \Phi_{T2} - \Phi_{S2} \\ &= \frac{2}{R_1\cos\alpha_1} - \frac{2\cos\alpha_1}{R_1} + \frac{2}{R_2\cos\alpha_2} - \frac{2\cos\alpha_2}{R_2}.\end{aligned} \tag{11}$$

To increase the optical power in the sagittal plane, a concave cylindrical mirror can be inserted between the grating and the focusing mirror, as shown in Fig. 3. The radius of the mirror, Rc, is defined as [7]

$$R_c = \left(\frac{1}{R_1\cos\alpha_1} - \frac{\cos\alpha_1}{R_1} + \frac{1}{R_2\cos\alpha_2} - \frac{\cos\alpha_2}{R_2}\right)^{-1}. \tag{12}$$

The off-axis angle α_2 of light incident on the focusing mirror varies with the wavelength. Therefore, for α_2 to be independent of the wavelength, the distance from the grating to the focusing mirror, L_{GF}, is constrained for the first-order approximation by the following relationship:

$$L_{GF} = L_{GC} + L_{CF} = R_2\cos\alpha_2. \tag{13}$$

The relationship in Eq. (13) also applies when using a toroidal focusing mirror. Therefore, the principles of astigmatism correction for the either configuration are nearly the same. However, it is difficult to fabricate a toroidal mirror but a cylindrical mirror can be off-the-shelf. In addition, with Eq. (13), Eq. (7) equals zero, and thus there is no variation in α_2.

3. Method comparison

3.1. Nonuniform astigmatism along the spectral direction

In the classic Czerny-Turner imaging spectrometer, the collimating and focusing mirrors introduce astigmatism because they are used off-axis in the tangential plane. However, the astigmatism from the collimating mirror is uniform at different wavelengths along the spectral direction, while that from the focusing mirror is nonuniform.

In configurations modified with either divergent illumination of the grating or with an added cylindrical lens, L_{GF} is usually set to approximately the tangential focal length of the focusing mirror, represented by $R_2\cos\alpha_2/2$. No measures are taken to avoid the nonuniform astigmatism introduced by the focusing mirror, so extra nonuniform astigmatism should be provided to correct astigmatism along the spectral direction. For the configuration with divergent illumination of the grating, Eq. (7) represents the nonuniform astigmatism along the spectral direction for the first-order approximation. The parameters L_{GF} and β are optimized to correct the nonuniform astigmatism, as explained in Section 2.2. For the configuration with the cylindrical lens, the nonuniform astigmatism is compensated by tilting the cylindrical lens at an angle δ and tilting the detector at an angle β along the spectral direction for the first-order approximation, as explained in Section 2.3.

For the configuration with the cylindrical mirror, L_{GF} is increased from $R_2\cos\alpha_2/2$ to $R_2\cos\alpha_2$ to let the focusing mirror introduce uniform astigmatism. The cylindrical mirror has an infinite raidus in the tangential plane, and a finite radius in the sagittal plane, so it offers nearly the uniform ability to correct astigmatism along the spectral direction, and it is suitable for correcting the introduced uniform astigmatism from focusing mirror.

Correcting astigmatism in the three modified configurations of the spectrometer is based on first-order approximation along the spectral direction, in which the angular spread $\Delta\theta$ that represents the disper-

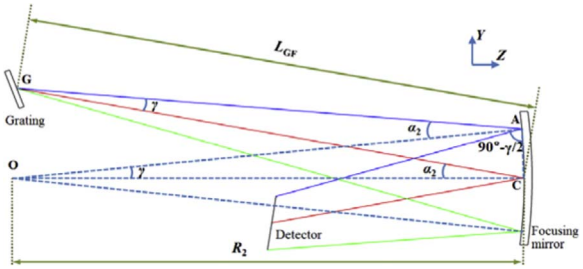

Fig. 4. Detailed ray tracing from the grating to the detector to achieve a uniform off-axis incident angle α_2 on the focusing mirror. Red rays represent the central wavelength and blue rays represent another wavelength whose diffraction angle is different from that of the central wavelength by γ. (For interpretation of the references to color in this figure legend, the reader is referred to the web version of this article.)

sion is limited.

We place an exact constraint on L_{GF} to let the focusing mirror introduce uniform astigmatism, which mathematically means that the off-axis angle α_2 is wavelength independent. A detailed ray tracing of beams from the grating to the focusing mirror to the detector is presented in Fig. 4. The grating works as a virtual stop in the tangential plane, and the dispersed rays from the grating are thought to have different FOVs in the tangential plane. The central wavelength rays (red) and the rays for another wavelength (blue) have the same off-angle α_2 on the focusing mirror. From the geometry of the triangle OAC in Fig. 4, we obtain the relationship:

$$\frac{OC}{\sin(90^\circ - \gamma/2)} = \frac{AC}{\sin\gamma}. \tag{14}$$

From the geometry of triangle GAC, we have

$$\frac{GC}{\sin(90^\circ - \gamma/2 + \alpha_2)} = \frac{AC}{\sin\gamma}. \tag{15}$$

From Eqs. (14) and (15), if GC equals L_{GF} and OC equals R_2, then

$$L_{GF} = R_2\cos\alpha_2 + R_2\sin\alpha_2\tan(\gamma/2). \tag{16}$$

To obtain the same α_2 at different wavelengths, the needed L_{GF} will vary. Only when α_2 and $\Delta\theta$ are small can Eq. (16) be simplified to Eq. (13) for the first-order approximation. Over a broadband spectral range, Eq. (13) is the constraint for L_{GF} at the central wavelength, while at the maximum or minimum wavelength, L_{GF} is related to $\Delta\theta$ as follows:

$$L_{GF} = R_2\cos\alpha_2 + R_2\sin\alpha_2\tan(\Delta\theta/4). \tag{17}$$

The difference in constraint for L_{GF} over the entire spectral range is very large and expressed as

$$\Delta L_{GF} = R_2\sin\alpha_2\tan(\Delta\theta/4). \tag{18}$$

Therefore, the spherical focusing mirror cannot introduce uniform astigmatism over a broadband wavelength range in any of the configurations because L_{GF} is fixed. In the configuration with the cylindrical mirror, the ability to correct astigmatism degrades as the wavelength bandwidth increases. In the configurations with divergent illumination of the grating and with the cylindrical lens, the techniques for correcting astigmatism are based on the first-order approximation as well, but the theoretical analysis of these configurations is complex. We quantitatively evaluate the performance of these corrective techniques along the spectral direction over different spectral ranges in Section 4.

3.2. Aberrations along the spatial direction

Figs. 2–4 present the optical layouts of the three modified configurations in the tangential plane, so only aberrations along the spectral direction are considered. The three modified configurations are applicable to imaging spectrometers with a pinhole entrance and linear sensor. This setup is used in the FD-OCT system or a whiskbroom

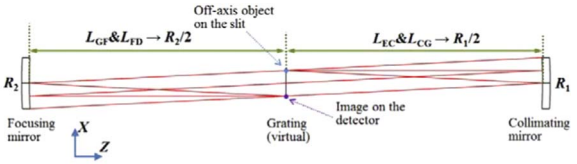

Fig. 5. Expanded optical layout of the classic Czerny-Turner imaging spectrometer in the sagittal view.

scanning instrument. For an imaging spectrometer with a slit entrance and area sensor, which provides not only spectral discrimination but also spatial discrimination, aberrations along the spatial direction also must be taken into consideration.

The collimating mirror collimates the rays from each FOV of the entrance slit in the sagittal plane before they go to the grating, where they are dispersed in the tangential plane. The area sensor captures the two-dimensional (2D) data, with 1D along the spectral direction and 1D along the spatial direction. The grating is a stop in the sagittal plane for the different FOVs from the entrance slit, and works as a virtual stop in the tangential plane for the dispersed rays diffracted from the grating which can be considered as different FOVs.

Fig. 5 shows the sagittal view of the classic Czerny-Turner imaging spectrometer, with the optical layout expanded at the grating. The distance between the entrance slit and the collimating mirror, L_{EC}, and the distance between the collimating mirror and the grating, L_{CG}, are equal to or approximately half the radius of the collimating mirror, R_1/2. In addition, the distance between the grating and the focusing mirror, L_{GF}, and that between the focusing mirror and the detector, L_{FD}, are equal to or approximately half the radius of the focusing mirror, R_2/2. While the collimating mirror and the focusing mirror are not tilted in the sagittal plane, the off-axis angles of the rays on these two spherical mirrors originate only from the off-axis object on the slit, which is the nonzero FOV. Off-axis angles in the sagittal plane are much smaller than the angles in the tangential plane. This asymmetrical configuration, which is the same as that in the tangential plane, automatically corrects coma. Astigmatism due to off-axis reflection in the sagittal plane is diffraction limited for an appropriate spatial extent (small off-axis angles). Therefore, for the modified configuration with divergent illumination of the grating, only the distance between each element varies and aberrations along the spatial direction are not a problem.

In the modified configuration with a cylindrical lens, L_{EC} and L_{CG} are still approximately R_1/2, while L_{GF} and L_{FD} approach R_2/2. The cylindrical lens is placed in the path of the focused beam from the focusing mirror, in front of the detector, and plays an important role in the sagittal plane. Fig. 6 shows a detailed optical layout of this configuration. The cylindrical lens is tilted at an angle δ about the X axis to compensate for the nonuniform astigmatism along the spectral direction. The tilt angle causes the imaging quality along the spatial direction to degrade as the FOV increases. Thus, it is difficult to correct aberrations along the spatial direction in this configuration.

In the modified configuration with a cylindrical mirror, the distance from the collimating mirror to the grating, L_{CG}, and the distance from the grating to the focusing mirror, L_{GF}, are stretched. The optical layout

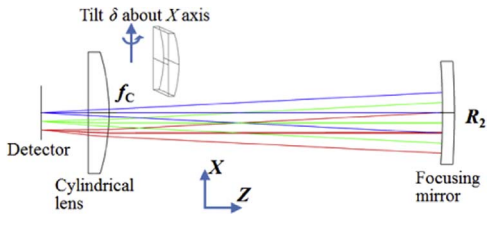

Fig. 6. Detailed optical layout of the modified configuration with a cylindrical lens in the sagittal view. The different colored rays indicate different FOVs along the spatial direction.

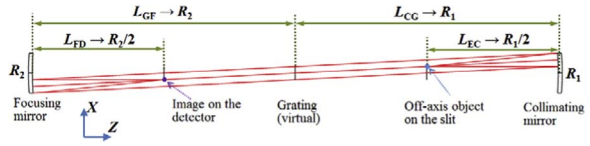

Fig. 7. Expanded optical layout of the modified configuration with a cylindrical mirror (not shown) in the sagittal view.

of this modified configuration in the sagittal view is shown expanded and without the cylindrical mirror in Fig. 7. The collimating mirror and focusing mirror are on-axis in the sagittal plane. When $L_{CG} \approx R_1$, the incident angle on the collimating mirror approaches zero for any FOV along the spatial direction. Similarly, when $L_{GF} \approx R_2$, the incident angle on the focusing mirror of rays from the same object on the entrance slit approaches zero for each wavelength (equal to any FOV along the spatial direction). According to the first-order approximation, to achieve zero off-axis angles in the sagittal plane, the distance from the grating to the spherical mirrors should be equal to twice the focal length of the spherical mirrors in the sagittal plane. Thus, L_{CG} and L_{GF} are defined by the following equations:

$$L_{CG} = R_1 \sec\alpha_1, \tag{19}$$

$$L_{GF} = R_2 \sec\alpha_2. \tag{20}$$

However, to achieve uniform off-axis angles on the focusing mirror along the spectral direction in the tangential plane, L_{GF} is constrained by Eq. (13) and L_{CG} is constrained by

$$L_{CG} = R_1 \cos\alpha_1. \tag{21}$$

When the entrance of the imaging spectrometer is a slit, the constraints for L_{CG} and L_{GF} conflict, but, fortunately, the off-axis angles α_1 and α_2 are usually just a few degrees. Therefore, when $L_{CG}=R_1$ and $L_{GF}=R_2$, a compromise is made with respect to the constraint of the off-axis angles along the spectral and spatial directions. In the sagittal plane, the off-axis angles at which the rays are incident on both the collimating mirror and the focusing mirror are approximately zero for any FOV of the slit. Thus, these two spherical mirrors introduce minor aberrations along the spatial direction, so the cylindrical mirror is inserted in the path of the collimated beam between the grating and the focusing mirror. The radius R_c of the cylindrical mirror in the sagittal plane is usually thousands of millimeters, so its impact on the nonzero FOV of the slit is almost the same as that on the zero FOV (similar to a pinhole entrance). The above analysis shows that aberrations along the spatial direction should not be an obstacle to improving the performance of a spectrometer with this configuration.

4. Design examples and ray tracing analysis

4.1. Benchmark and off-the-shelf optics

In this section, we present the designs of the imaging spectrometer with the three modified configurations discussed in Section 3, with a spectral resolution of 0.1 nm as the target for all three.

We started with the classic Czerny-Turner imaging spectrometer as the benchmark and used only off-the-shelf optics in our designs. The central wavelength λ_0 was 800 nm because the near-infrared is the region of interest in FD-OCT systems. The grooves of the grating (53-*-035R; Richardson Gratings, Rochester, NY, USA) had a spacing of d=1.2 μm. The angle of incidence on the grating was −8°, the diffraction angle was −31.66° at λ_0, and m=−1 in Eq. (2); this value guarantees a sufficient spectral range. The collimating and focusing mirrors both had the same radius of curvature of 200 mm and were available in three sizes: diameter=12.7, 25.4, or 50.8 mm (05DC200ER.2, 10DC200ER.2, 20DC200ER.2, respectively; Newport Corporation, Irvine, CA, USA). The stop was set on the 10-mm-diameter grating, so the imaging spectrometer had a stop of f/10. Thus, the spherical mirror chosen depended on the requirement of a clear aperture. The off-axis angles α_1 of the collimating mirror and α_2 of the focusing mirror were set to −5° and −8° initially. The resolution of the detector with the linear sensor was 1×1024, 1×2048, or 1×4096 [L104-1k and L104-2k (Basler Vision Technologies) and spL4096–50 km (Basler AG, Ahrensburg, Germany), respectively], and that of the detector with the area sensor (HCC-1000BGE, Simi Reality Motion Systems GmbH, Unterschleißheim, Germany) was 1024×1024, all of which are consistent with a pixel size of 10 μm. The selection of the detector depended on the spatial extent and spectral range requirements. The grating was chosen to provide, together with the radius R_2 of the focusing mirror, the appropriate angular spread $\Delta\theta$ so that the selected detector achieved a spectral resolution of 0.1 nm. Following Eq. (4), for configurations with a point FOV, the linear sensor with 1×1024 resolution was used for the 100-nm wavelength bandwidth, that with 1×2048 resolution was used for the 200-nm wavelength bandwidth, and that with 1×4096 resolution was used for the 400-nm wavelength bandwidth. The lateral magnification of −1 was achieved because the radii of the collimating and focusing mirrors were the same. For configurations with a 1D FOV, the area sensor with 1024×1024 resolution was used for the 100-nm wavelength bandwidth over a 10-mm spatial extent along the entrance slit.

4.2. Design results and imaging quality evaluation

We used OpticStudio 16 SP2 software (Zemax LLC, Kirkland, WA, USA) to design the configurations. In our designs, the tilt angle of each element and the distance between each element were varied, and the RMS spot radius throughout the spectral range and spatial FOVs was set as the merit function during optimization. We designed the three modified spectrometer configurations separately for the point FOV with a wavelength bandwidth of 100, 200, or 400 nm, and for a wavelength bandwidth of 100 nm over a spatial extent of 10 mm along the entrance slit.

The parameters of the resulting designs are listed in Table 1. For configuration 2, we used an off-the-shelf cylindrical lens made of BK7 with a focal length of 100 mm and a central thickness of 5.2 mm (LJ1567L1-C; Thorlabs, Newton, NJ, USA). For configuration 3, the optimized radius of the cylindrical mirror was ~3520 mm for each design, so we used an off-the-shelf concave cylindrical mirror with a radius of 3500 mm (CCLM3500; M-optics, Nanjing, China) and then re-optimized the designs. For a broader wavelength bandwidth, we used a focusing mirror with a larger diameter and a detector with higher resolution. In addition, as the dimension of each element increased in the designs, the off-axis angle α_2 was increased to avoid obstructing the rays, thus causing α_1 to be increased correspondingly to satisfy Eq. (1) for coma correction.

First, we evaluated the performance of the three modified configurations with a point FOV over $\Delta\lambda$ of 100, 200, and 400 nm. Fig. 8 shows that as $\Delta\lambda$ increases, the performance of each configuration degrades. For the configuration with divergent illumination of the grating and the configuration with a cylindrical mirror, the maximum allowable $\Delta\lambda$ is 200 nm, as shown in Fig. 8(b) and (h). However, for the configuration with a cylindrical lens, the maximum allowable $\Delta\lambda$ reaches as high as 400 nm, as seen in Fig. 8(f), where it is twice that of the other two configurations.

The differences in $\Delta\lambda$ are attributed to the different schemes for compensation of nonuniform astigmatism along the spectral direction, as explained in Section 3.1. In the configuration with a cylindrical mirror, to avoid nonuniform astigmatism on the focusing mirror, L_{GF} is "stretched" or increased according to Eq. (13) and then the nearly uniform astigmatism is compensated for by the cylindrical mirror. However, the first-order approximation fails to work for a broader $\Delta\lambda$ and, thus, the constraint difference for L_{GF} over the entire spectral range is very large, as indicated by Eqs. (17) and (18). The minimum

Table 1
Optimized parameters for different configurations of the imaging spectrometer.

Configuration[a]	1	2	3	1	2	3	1	2	3	1	2	3
Spectral range (nm)	750–850			700–900			600–1000			750–850		
Detector resolution (pixels)	1×1024			1×2048			1×4096			1024×1024		
α_1 (°)	−5	−5	−6	−5	−5	−6	−7	−5	−8	−5	−5	−6
α_2 (°)	−8	−8	−12	−8	−8	−12	−11	−10	−20	−8	−8	−12
α_3 (°)	–	–	−15	–	–	−15	–	–	−20	–	–	−15
β (°)	12.69	3.81	23.47	12.56	3.74	23.43	18.44	5.00	36.98	15.24	9.85	23.53
δ (°)	–	−17.20	–	–	−17.66	–	–	−17.52	–	–	15.73	–
L_{EC} (mm)	91.01	100	100	90.96	100	100	87.80	100	100	90.79	100	100
L_{CG} (mm)	100	100	200	100	100	200	100	100	200	100	100	200
L_{GF} (mm)	108.33	100	–	104.74	100	–	100	100	–	137.94	100	–
L_{FD} (mm)	110.45	100.36	97.15	110.70	100.36	97.36	116.35	100.30	94.39	110.49	102.37	97.20
L_{FC} (mm)	–	83.74	–	–	83.85	–	–	81.59	–	–	85.54	–
L_{GC} (mm)	–	–	100	–	–	100	–	–	100	–	–	100
L_{CF} (mm)	–	–	96.12	–	–	96.72	–	–	92.33	–	–	100
f_c (mm)	–	100	–	–	100	–	–	100	–	–	100	–
R_c (mm)	–	–	−3500	–	–	−3500	–	–	−3500	–	–	−3500

[a] configuration 1: configuration with divergent illumination of the grating, configuration 2: configuration with a cylindrical lens, configuration 3: configuration with a cylindrical mirror.

and maximum constraints on L_{GF}, based on calculations using Eq. (17), are listed in Table 2. When the spectral range increases to >200 nm, nonuniform astigmatism is unavoidable regardless of the value of L_{GF}. The other two configurations compensate for nonuniform astigmatism. In the configuration with divergent illumination of the grating, L_{GF} and the tilt angle β of the detector are optimized to compensate for the wavelength-dependent astigmatism. In the configuration with the cylindrical lens, the tilt angle δ of the cylindrical lens is a variable that can be optimized. Although these two astigmatism compensation schemes are based on the first-order approximation, the latter configuration can afford a broader spectral range according to the comparison of the design examples in Fig. 8(d)–(f). This achieves a $\Delta\lambda$ of 400 nm with near diffraction-limited performance in our design examples.

Table 2
L_{GF} parameters for the configuration with a cylindrical mirror for different $\Delta\lambda$..

$\Delta\lambda$ (nm)	α_2 (deg)	$\Delta\theta$ (deg)	Minimum L_{GF} (mm)	Maximum L_{GF} (mm)	ΔL_{GF} (mm)	Optimized L_{GF} (mm)
100	12	5.59°	195.63	196.64	1.01	196.12
200	12	11.21°	195.63	197.67	2.04	196.72
400	20	22.68°	187.94	194.73	6.79	192.33

The performances of the three modified configurations with 1D FOV are compared in Fig. 9, which presents the RMS spot radius as a function of wavelength for different FOVs. Rays were traced from points along the entrance slit in the optimized designs only for the zero FOV (columns 2–4 of Table 1). In Fig. 9(a), the curves for the nonzero

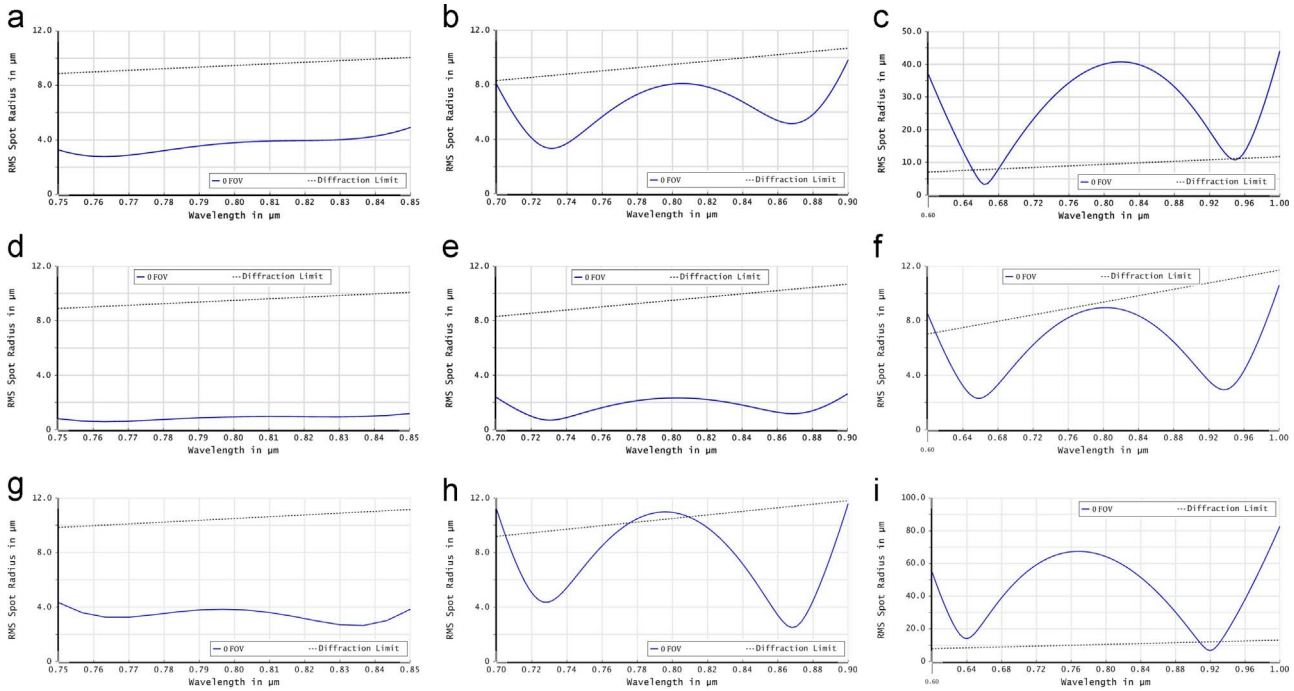

Fig. 8. RMS spot radius as a function of wavelength for the three configurations of the imaging spectrometer with a point FOV. (Left column) Configuration with divergent illumination of the grating over a wavelength bandwidth ($\Delta\lambda$) of (a) 100 nm, (b) 200 nm, (c) 400 nm. (Middle column) Configuration with a cylindrical lens over a $\Delta\lambda$ of (d) 100 nm, (e) 200 nm, (f) 400 nm. (Right column) Configuration with a cylindrical mirror over a $\Delta\lambda$ of (g) 100 nm, (h) 200 nm, (i) 400 nm.

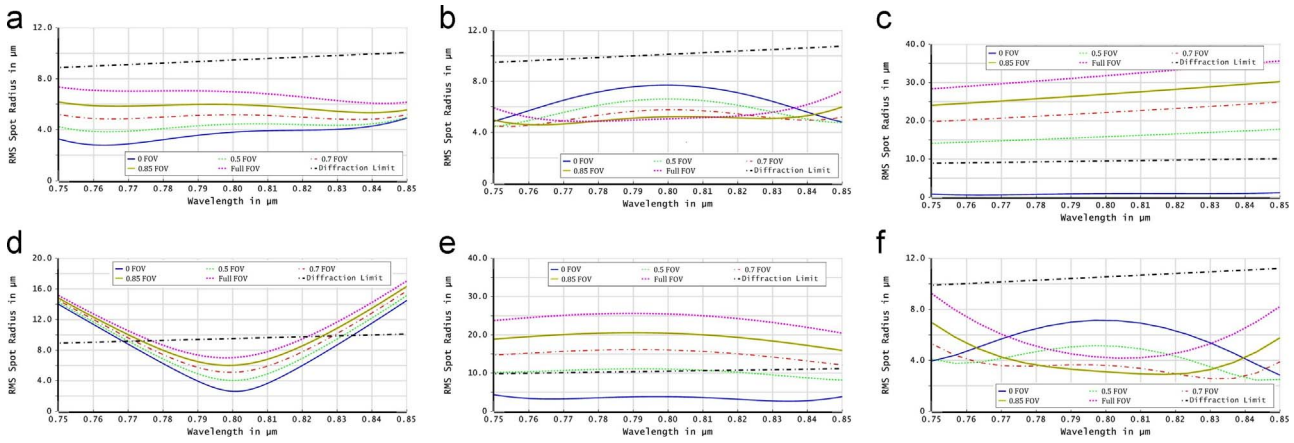

Fig. 9. RMS spot radius as a function of wavelength for the imaging spectrometer with a 1D FOV over a wavelength bandwidth ($\Delta\lambda$) of 100 nm. (Left column) Configuration with divergent illumination of the grating in the optimized designs of (a) only for zero FOV and (b) considering 1D FOV. (Middle column) Configuration with a cylindrical lens in the optimized designs of (c) only for zero FOV and (d) considering 1D FOV. (Right column) Configuration with a cylindrical mirror in the optimized designs of (e) only for zero FOV and (f) considering 1D FOV.

FOVs and the zero FOV for the configuration with divergent illumination of the grating are very close together and show diffraction-limited performance (column 2 of Table 1). This phenomenon is inconsistent with the ability of the configuration to autocorrect aberrations in the sagittal plane. In Fig. 9(c) and (e), the curves for nonzero FOVs and the zero FOV are farther apart (columns 3 and 4 of Table 1), probably a result of the effect of the added cylindrical lens and cylindrical mirror in these two configurations. Fig. 9(b) shows that after optimization with 1D FOV of the configuration with divergent illumination of the grating, a minor change is observed (column 11 of Table 1). Diffraction-limited performance can also be achieved in the configuration with a cylindrical mirror (column 13 of Table 1), as shown in Fig. 9(f). Compared with Fig. 9(c), and the curves in Fig. 9(d) are close, but aberrations remain uncorrected for marginal wavelengths for the configuration with a cylindrical lens. The tilt angle δ of the cylindrical lens changed from −17.20 to 15.73° after optimization. As discussed in Section 3, the cylindrical lens is tilted to compensate for the wavelength-dependent astigmatism along the spectral direction, but the imaging quality along the spatial direction degrades as the FOV increases, as demonstrated by the separated curves in Fig. 9(c). As the sign of δ changes in our designs, nearly uniform aberration correction along the spatial direction is achieved, but astigmatism correction is invalidated along the spectral direction. In the configuration with the cylindrical lens, aberration correction in the tangential plane conflicts with that in the sagittal plane, making this configuration unsuitable for an imaging spectrometer with a 1D FOV.

A comparison of Figs. 8 and 9 shows that the configuration with a cylindrical lens corrects astigmatism along the spectral direction over a wide spectral range, but its performance degrades rapidly when the FOV along the spatial direction increases.

4.3. Distortion and ray tracing analysis

To perform a comprehensive evaluation of an imaging spectrometer, distortion, including spectral nonlinearity, smile, and keystone, must be included [21].

The goal of our designs is a uniform spectral resolution of 0.1 nm over the spectral range; however, usually the relationship between the pixel number of the detector and wavelength is a third-order polynomial [22]:

$$\lambda_p = I + C_1 p + C_2 p^2 + C_3 p^3, \tag{22}$$

where λ_p is the wavelength of pixel p, I is the wavelength of pixel 0, C_1 is the first coefficient (nm/pixel), C_2 is the second coefficient (nm/pixel^2), and C_3 is the third coefficient (nm/pixel^3). Spectral nonlinearity is then defined as

$$\delta\lambda = \lambda_p - I - C_1 p. \tag{23}$$

We performed ray tracing for the three configurations with point FOV over a $\Delta\lambda$ of 200 nm (columns 5–7 in Table 1) to calculate spectral nonlinearity. Sampling wavelengths were created in the wavelength range of 700–900 nm using a 10-nm interval. Rays were traced across the 100×100 grids on the stop (grating) for each wavelength and their Y coordinates on the linear sensor were recorded. Then, the centroid of the spots at each wavelength was calculated. The centroids were used to obtain spectral nonlinearity using Eqs. (22) and (23). Fig. 10 shows the spectral nonlinearity curves for the three configurations. The wavelengths are distinguished by color grading the curves. The configuration with the cylindrical mirror had the smallest spectral nonlinearity. We also calculated the spectral nonlinearity of the three configurations with 1D FOV over a $\Delta\lambda$ of 100 nm and found that it slightly increases as FOV increases. However, the configuration with the cylindrical mirror still had the best performance.

Distortion over wavelength and field was calculated for the imaging spectrometer with 1D FOV. Smile distortion occurs when the entrance slit is imaged onto the area sensor but is curved along the spatial direction. Keystone distortion occurs when the FOV from the entrance slit is dispersed onto the area sensor, and the dispersed spots are not aligned but curved along the spectral direction.

Next, we compared the designs of the configurations with divergent illumination of the grating and with a cylindrical mirror (columns 11 and 13 of Table 1). The entrance slit was separated equally into 21 sampling FOVs, and the spectrum from 750 to 850 nm was divided into

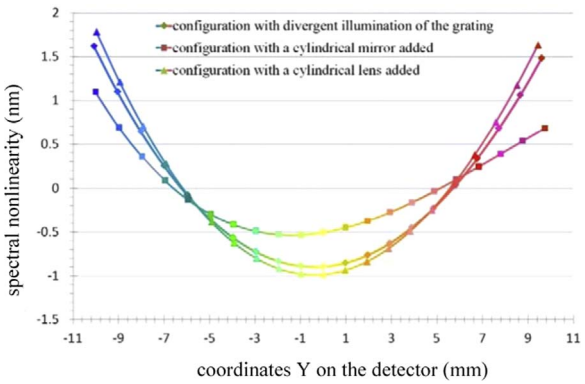

Fig. 10. Spectral nonlinearity curves for three configurations with point FOV over $\Delta\lambda$ of 200 nm.

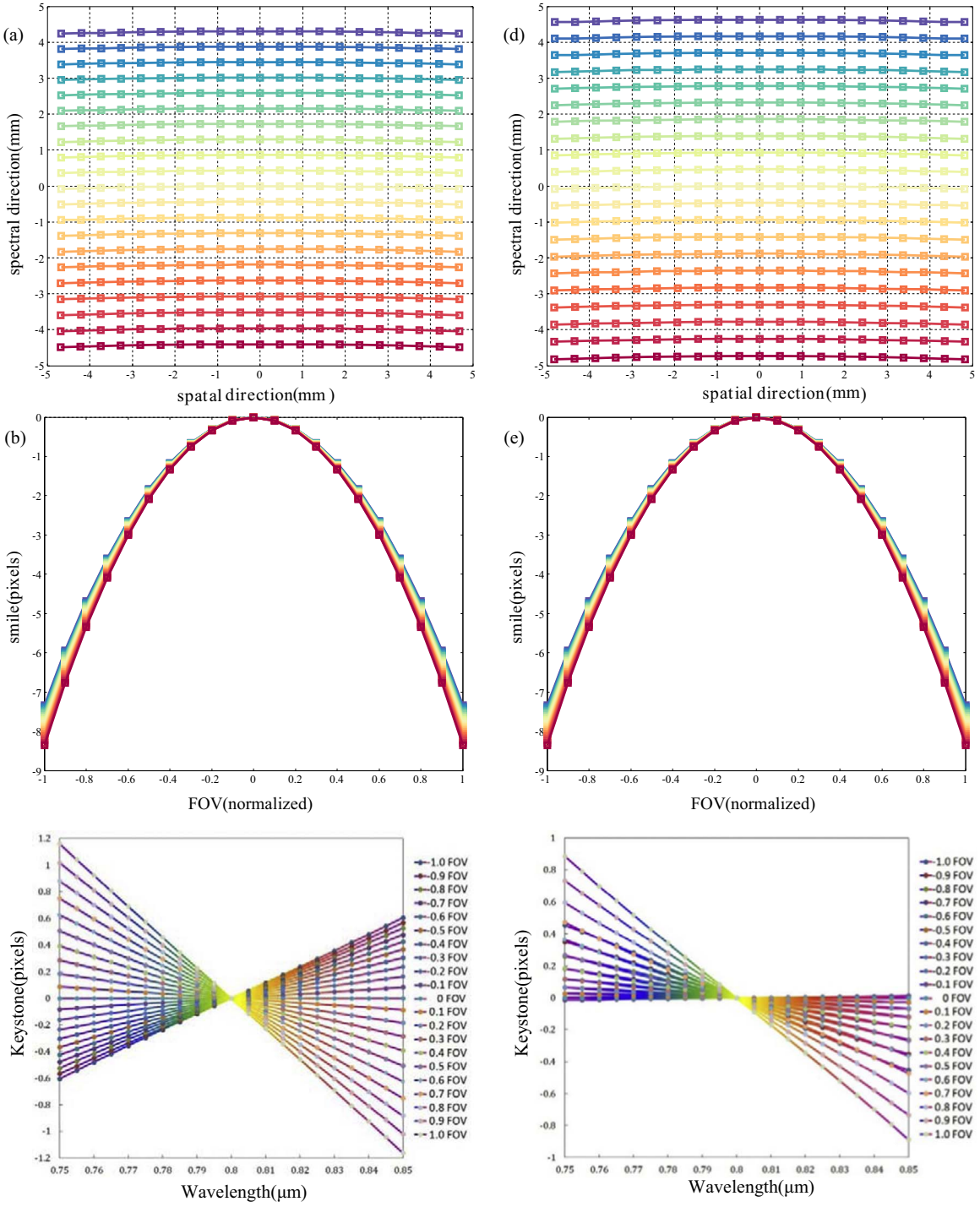

Fig. 11. Distortion calculations at different wavelengths and FOVs for two designs of the 1D imaging spectrometer. (a) Ray tracing on the area sensor, (b) smile, and (c) keystone for the configuration with divergent illumination of the grating. (d) Ray tracing on the area sensor, (e) smile, and (f) keystone for the configuration with a cylindrical mirror.

21 sampling wavelengths using a 10-nm interval. Rays from each FOV at each wavelength were traced across the 100×100 grids on the stop (grating) and the centroid of the spots was calculated. Ray tracing results on the area sensor are shown in Fig. 11(a) and (d), where the dots and squares represent the centroids for each FOV at each wavelength. Centroids at different wavelengths have different colors, and centroids at the same wavelength are connected by lines to obtain the image of the entrance slit. There is smile because the lines are curved.

Smile and keystone were calculated based on the coordinates of the centroids from the ray tracing, and their curves are displayed in Fig. 11(b) and (c) and (e) and (f). For the full FOV, smile reaches as high as 80 μm in both configurations with a 10-μm pixel size. Therefore, the imaging spectrometer should be calibrated for smile. Keystone in the configuration with the cylindrical mirror is within one pixel and is smaller than that in the configuration with divergent illumination of the grating.

Thus, to design an imaging spectrometer with a 1D FOV, the configuration with divergent illumination of the grating and the configuration with a cylindrical mirror are two options in which only off-the-shelf optics can be used. The latter configuration is superior with respect to spectral nonlinearity and keystone. However, no extra

elements are needed for the configuration with divergent illumination of the grating and it still provides acceptable performance; thus, this configuration is a good and simple option.

In addition to the three modified configurations, we also evaluated a configuration that contained a toroidal focusing mirror because it is a commonly used technique. Astigmatism correction in this configuration is similar to that used for the configuration with the cylindrical mirror, whereby the distance from the grating to the focusing mirror, L_{GF}, is stretched to approximately $R_2\cos\alpha_2$. Detailed examples of design and ray tracing analysis are not presented here because this configuration is not the topic of this paper. However, the performance of the configuration with the toroidal focusing mirror was similar to that of the configuration with the cylindrical mirror.

5. Conclusion

We compared different techniques for correcting astigmatism in the Czerny-Turner imaging spectrometer using only off-the-shelf optics. First, we assessed three modified configurations—one with divergent illumination of the grating, one with a cylindrical lens added, and one with a cylindrical mirror added—by comparing their ability to correct aberration along the spectral direction and the spatial direction. On the basis of theoretical analysis, we made design examples of the three modified configurations, using the classic Czerny-Turner imaging spectrometer with fixed specifications as the benchmark, setting the spectral resolution of 0.1 nm as the common criterion and using a pixel size of 10 μm for all three configurations. We comprehensively evaluated the performance of each design. For a point FOV, the configuration with the cylindrical lens can be used with the maximum spectral range, i.e., a bandwidth of 400 nm centered at 800 nm. However, this configuration does not work with a 1D FOV because of its limited ability to correct aberration along the spatial direction. The divergent illumination of the grating and the cylindrical mirror configurations work in the wavelength bandwidth of 200 nm for a point FOV and equally show the ability to correct aberration along the spectral direction and the spatial direction. In addition, these two configurations achieve near diffraction-limited imaging quality over a 100-nm bandwidth and 10-mm spatial extent along the entrance slit. The configuration with the cylindrical mirror performed better with respect to distortion, including spectral nonlinearity, smile, and keystone. This paper should help decide on a cost-effective design of an imaging spectrometer using off-the-shelf optics depending on its application and the required specifications.

One can request the ZEMAX design files, ray tracing ZPL file, and MATLAB codes for distortion calculations from Dr. Qun Yuan at karmen86913@gmail.com.

Acknowledgments

This research was funded by the National Natural Science Foundation of China (61505080 and 61377015), the Natural Science Foundation of Jiangsu Province (BK20150788), and the Open Research Fund of the Jiangsu Key Laboratory of Spectral Imaging and Intelligent Sense (3091601410402).

References

[1] M. Czerny, A. Turner, On the astigmatism of mirror spectrometers, Z. Phys. 61 (1930) 792–797.
[2] A.B. Shafer, L.R. Megill, L. Droppleman, Optimization of the Czerny–Turner spectrometer, J. Opt. Soc. Am. 54 (7) (1964) 879–886.
[3] M.R. Torr, D.G. Torr, Compact imaging spectrograph for broadband spectral simultaneity, Appl. Opt. 34 (34) (1995) 7888–7898.
[4] J. Schwider, L. Zhou, Dispersive interferometric profilometer, Opt. Lett. 19 (13) (1994) 995–997.
[5] J. Huang, et al., Measurement of a multi-layered tear film phantom using optical coherence tomography and statistical decision theory, Biomed. Opt. Express 5 (12) (2014) 4374–4386.
[6] K.S. Lee, K.P. Thompson, J.P. Rolland, Broadband astigmatism corrected Czerny–Turner spectrometer, Opt. Express 18 (22) (2010) 23378–23384.
[7] Y. Tang, et al., Design of visible-ultraviolet cylinder mirror imaging spectrometer, Acta Opt. Sin. 33 (3) (2013) 0330004.
[8] E.S. Voropai, I.M. Gulis, A.G. Kupreev, Astigmatism correction for a large-aperture dispersive spectrometer, J. Appl. Spectrosc. 75 (1) (2008) 150–155.
[9] C. Chrystal, K.H. Burrell, N.A. Pablant, Straightforward correction for the astigmatism of a Czerny–Turner spectrometer, Rev. Sci. Instrum. 81 (2) (2010) 023503.
[10] X. Ge, S. Chen, Y. Zhang, H. Chen, P. Guo, T. Mu, J. Yang, Z. Bu, Broadband astigmatism-corrected spectrometer design using a toroidal lens and a special filter, Opt. Laser Technol. 65 (2015) 88–93.
[11] X. Zhong, Y. Zhang, G. Jin, High performance Czerny-Turner imaging spectrometer with aberrations corrected by tilted lenses, Opt. Commun. 338 (2015) 73–76.
[12] M.D. Mouriz, E.L. Lago, X. Prieto-Blanco, H. González-Núñez, R. de la Fuente, Schwarzschild spectrometer, Appl. Opt. 50 (16) (2011) 2418–2424.
[13] S.H. Kim, H.J. Kong, S. Chang, Aberration analysis of a concentric imaging spectrometer with a convex grating, Opt. Commun. 333 (2014) 6–10.
[14] M. Futamata, T. Takenouchi, K. Katakura, Highly efficient and aberration-corrected spectrometer for advanced Raman spectroscopy, Appl. Opt. 41 (22) (2002) 4655–4665.
[15] Q. Xue, S. Wang, F. Lu, Aberration-corrected Czerny-Turner imaging spectrometer with a wide spectral region, Appl. Opt. 48 (1) (2009) 11–16.
[16] D.R. Austin, T. Witting, I.A. Walmsley, Broadband astigmatism-free Czerny-Turner imaging spectrometer using spherical mirrors, Appl. Opt. 48 (19) (2009) 3846–3853.
[17] T. Yang, J. Zhu, W. Hou, G. Jin, Design method of freeform off-axis reflective imaging systems with a direct construction process, Opt. Express 22 (2014) 9193–9205.
[18] T. Yang, J. Zhu, X. Wu, G. Jin, Direct design of freeform surfaces and freeform imaging systems with a point-by-point three-dimensional construction-iteration method, Opt. Express 23 (2015) 10233–10246.
[19] J. Reimers, J.P. Rolland, Spectral full-field displays for spectrometers, Class. Opt. 5 (2014) ITh3A.
[20] R.G. Sellar, G.D. Boreman, Classification of imaging spectrometers for remote sensing applications, Opt. Eng. 44 (1) (2005) 013602.
[21] P. Mouroulis, Spectral and spatial uniformity in pushbroom imaging spectrometers, Imaging Spectrom. V Proc. SPIE 3753 (1999) 133–141.
[22] O.Optics, Inc., Calibrating the Wavelength of the Spectrometer, available at ⟨http://www.oceanoptics.cn/system/files/documents/calibrating_wavelength_of_spectrometer.pdf⟩.